JOURNAL OF SOLID STATE CHEMISTRY **140,** 38–45 (1998)
ARTICLE NO. SC987820

On the Spinel Precipitation in Al-Doped $Ni_{1-x}O$

S. R. Wang and P. Shen[1]

Institute of Materials Science and Engineering, National Sun Yat-sen University, Kaohsiung, Taiwan Republic of China

Received November 7, 1997; in revised form March 6, 1998; accepted March 12, 1998

The $Ni_{1-x}O/NiAl_2O_4$ (69:1 molar ratio) composite fired at 1873 K for 1–80 h and then slowly cooled or water quenched in air was studied by X-ray diffraction and electron microscopy to clarify the stoichiometry, microstructures, and formation mechanism of spinel precipitates in Al-doped $Ni_{1-x}O$. Expulsion of Al^{3+} during slow cooling caused the formation of stoichiometric $NiAl_2O_4$ precipitates which contained $\{110\}$ domain boundaries of spinelloid nature and were of the same size regardless of the firing time at 1873 K. Instead of growing at $NiAl_2O_4$ seeds, the spinel precipitate nucleated from dislocations (line vector parallel to $\langle 100\rangle$), hence with $\{100\}$ rather than close-packed $\{111\}$ as the habit plane. The $\{100\}$ interface is coherent given that the lattice parameter for $NiAl_2O_4$ is almost exactly twice that of $Ni_{1-x}O$. On the basis of diffusion data reported for Al-doped $Ni_{1-x}O$ single crystals, we suggest that below 1473 K, moving of some Al^{3+} dopant from octahedral to interstitial tetrahedral sites caused the spinel nucleation to preferentially occur at dislocation cores with beneficial higher diffusivity and lower activation energy for defect clustering.

1. INTRODUCTION

Wüstite ($Fe_{1-x}O$) is an oxide with the rock salt structure that shows a considerable degree of nonstoichiometry ($x \leq 0.15$ (1)), defect clustering, and ordering (2). Long-range ordering of such defects caused the formation of superstructures such as the spinel P″ and P‴ phases (3, 4). In addition, the P′ phase, originally interpreted as a $2.6 \times 2.6 \times 2.6$ supercell of wüstite (5), gave diffuse X-ray scattering patterns consistent with a paracrystalline array of defects embedded in the rock salt substructure (6). (The paracrystalline distribution is such that the longitudinal spacing between defects tends to be maintained fairly constant but relative lateral translations may occur more variably.) When these lateral translations are suppressed, the superlattice P″ phase appears (6).

In contrast to wüstite, busenite ($Ni_{1-x}O$), also with the rock salt structure, has very small x (ca. 0.001 at 1773 K (7)) and the occurrence of defect clustering is uncertain whether from the theoretical point of view (8, 9) or based on experimental results (10–14). There is, however, clearer experimental evidence of defect clustering in cation-doped $Ni_{1-x}O$. For example, (Zr, Y)-codoped or Zr-doped $Ni_{1-x}O$ gave diffraction patterns consistent with a paracrystalline ordered state which developed subsequently into a spinel structure upon annealing at 1573 and 1873 K (15, 16). Defect chemistry equations were proposed to account for the stabilization effect of Zr on defect clusters (15, 16).

Al-doped $Ni_{1-x}O$ was also found to have spinel precipitates at relatively low temperatures, and the defect speciation of the dopant as indicated by diffusivity data is of particular interest (17). Briefly, the ^{63}Ni tracer self-diffusion in Al-doped $Ni_{1-x}O$ single crystals (17) indicated that at temperatures above 1473 K, singly charged Ni^{3+}–vacancy pairs form associates with Al dopant ions with a binding energy of 1.2 eV. Below 1473 K some of the Al dopant was precipitated as spinel platelets, presumed to have the $NiAl_2O_4$ composition, which were observed to be coherent with respect to the $Ni_{1-x}O$ matrix on the basis of electron diffraction lattice parameters (17).

The original motivation for this research was to establish the nature of planar defects in the spinel precipitates of Al-doped $Ni_{1-x}O$. We intended also to prove by annealing and cooling experiments that the precipitates were nucleated rapidly at dislocations upon cooling and hence the absence of any intermediate paracrystalline state. Instead, platelets were formed on $\{001\}$: pure $Ni_{1-x}O$ is known to have dislocations with $\langle 001\rangle$ line vector (18). $NiAl_2O_4$ seeds were added to ensure that the Al-doped $Ni_{1-x}O$ is saturated with respect to the $NiAl_2O_4$ component and to study whether the seeds act as growth sites.

2. EXPERIMENTAL

The $Ni_{1-x}O$ (99.995%, Cerac) and Al_2O_3 (99.9%, Cerac) powders in 1:1 molar ratio were ball (Al_2O_3) milled in deionized water, oven dried at 373 K, and then reacted at 1373 K for 3 h to prepare stoichiometric $NiAl_2O_4$ spinel powders. Powder mixture batches were then prepared from $Ni_{1-x}O$ and $NiAl_2O_4$ (69:1 molar ratio) by ball milling and

[1]To whom correspondence should be addressed.

0022-4596/98 $25.00

oven drying as described. The powder mixture was then die-pressed at 650 MPa to form pellets ca. 5 mm in diameter and 1 mm in thickness. The pellets were fired at 1873 K for 1, 20, 40, 60, and 80 h in an open-air furnace and cooled in the furnace (5°C/min). The pellet fired at 1873 K for 1 h was also water quenched for comparison with those that were cooled in the furnace. The oxygen partial pressure was presumably 0.2 atm given the open-air furnace. X-ray diffraction (XRD, Cu$K\alpha$, 35 kV, 25 mA at 0.05° and 20 sec per step up to 2θ angle 145°) was used to identify the phases. The calculated lattice parameters from each d-spacing were plotted against $\cos^2\theta/\sin\theta$ and extrapolated to $\theta = 90°$ to obtain the precise lattice parameter a_0 (19), which can help tell if the precipitates are stoichiometric spinels or not, as in the case of the Zr-doped system (15).

The fired $Ni_{1-x}O/NiAl_2O_4$ composites were argon-ion milled to electron transparency and studied by transmission electron microscopy (TEM, JEOL 200CX at 200 kV and 3010 at 300 kV) coupled with energy-dispersive X-ray (EDX) analysis at 200 kV. Bright-field image (BFI), dark-field image (DFI), and selected-area diffraction (SAD) patterns were taken to identify phases and defects. Scanning electron microscopy (SEM, JSM-6400 at 20 kV) was used to study the thermally etched surface of the fired specimens.

3. RESULTS

3.1. Furnace Cooling

An SEM image of the $N_{69}S_1$ sample fired at 1873 K for 20–80 h and then cooled in the furnace shows the inter- and intragranular $NiAl_2O_4$ spinel particles in the $Ni_{1-x}O$ matrix (Fig. 1). The $Ni_{1-x}O$ grains showed precipitates which remained the same size for all firing times (Fig. 1),

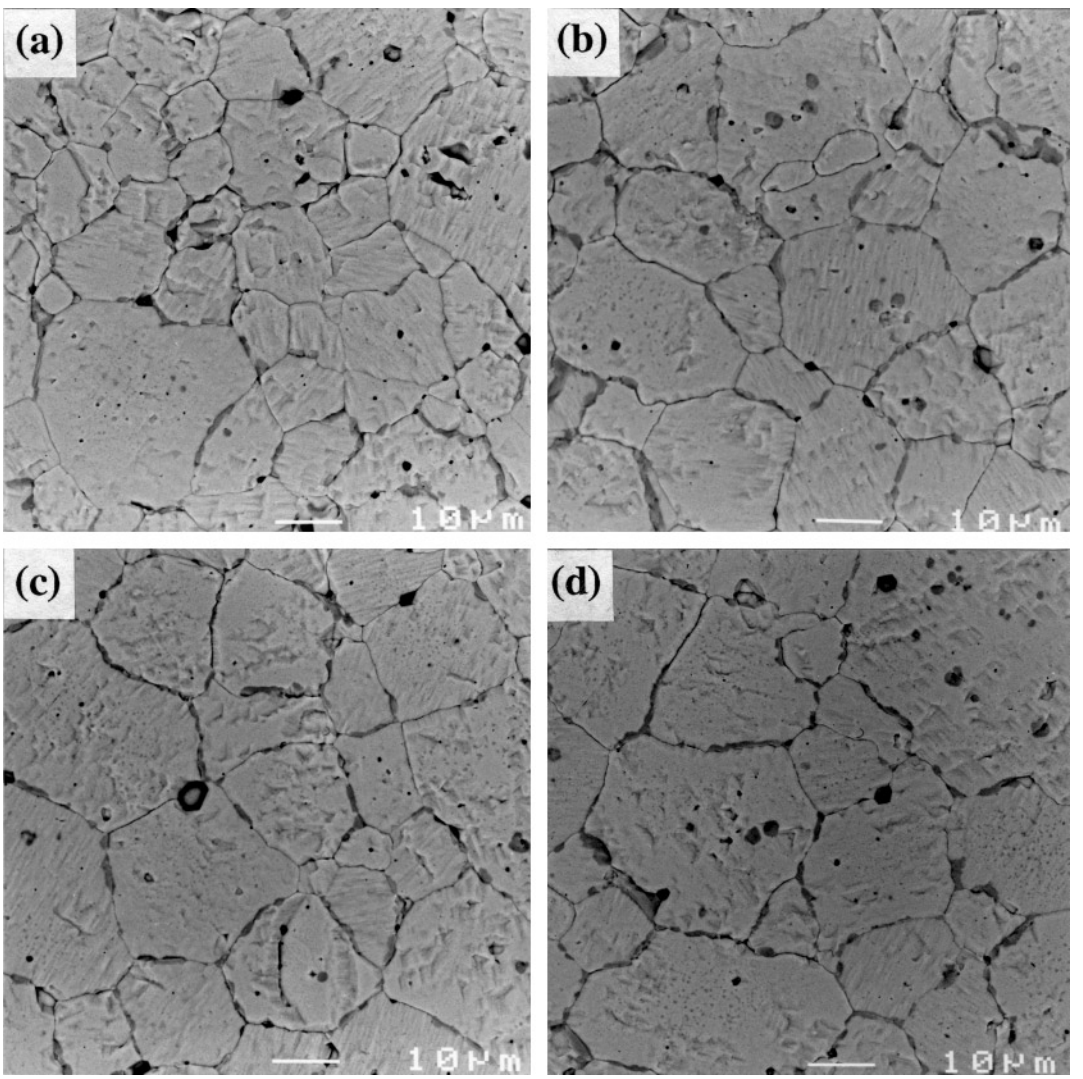

FIG. 1. SEM of the $NiAl_2O_4$ spinel particles located at and away from $Ni_{1-x}O$ grain boundaries for the $N_{69}S_1$ sample fired at 1873 K for (a) 20, (b) 40, (c) 60, and (d) 80 h. Note that the fine precipitates remain the same size.

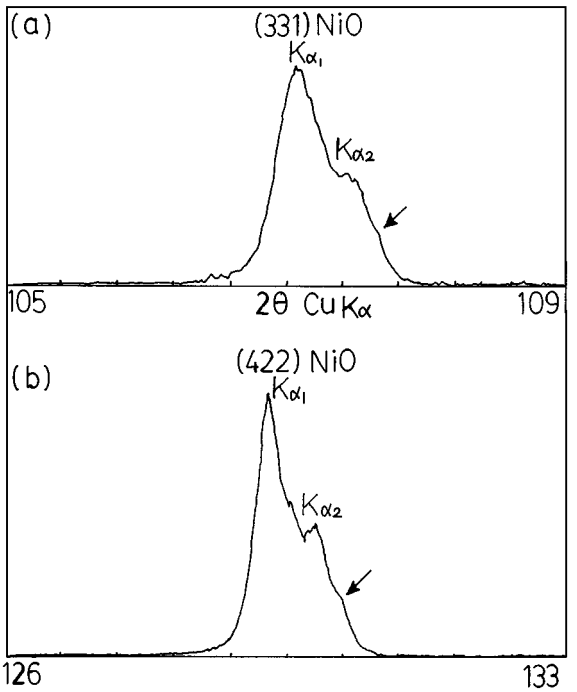

FIG. 2. XRD peaks of the $Ni_{1-x}O$ phase ($a_0 = 0.4177$ nm): (a) (331) and (b) (422), showing shoulders due to stoichiometric $NiAl_2O_4$ particles with $a_0 = 0.8048$ nm. $N_{69}S_1$ sample fired at 1873 K for 20 h and furnace-cooled.

indicating they were formed upon cooling rather than at 1873 K.

Step scanning of the XRD peaks (331) and (422) showed a predominant $Ni_{1-x}O$ phase ($a_0 = 0.4177$ nm according to the a_0 vs $\cos^2\theta/\sin\theta$ plot) and a single shoulder due to the stoichiometric $NiAl_2O_4$ phase with $a_0 = 0.8048$ nm (Fig. 2). This shoulder is nearly one-quarter of the intensity of the main peak and thus must be contributed predominantly from the spinel precipitates rather than the much smaller fraction of spinel seeds (1.4 mol%, i.e., 2.8 wt%). Thus both the seeds and the precipitates are the spinel phase of stoichiometric composition.

TEM study of the annealed samples further indicated the intragranular spinel particles were predominantly coalesced and rotated to fall into parallel epitaxy with respect to the $Ni_{1-x}O$ grain (20). The fine spinel precipitates also showed parallel epitaxy with respect to the grain and had a $\{100\}$ habit plane as represented by the sample fired at 1873 K for 60 h (Fig. 3). A point-count EDX spectrum (not shown) indicated the $Ni_{1-x}O$ matrix is nearly free of Al content and the spinel precipitates appeared to have a lower Al/Ni count ratio than the $NiAl_2O_4$ seeds due to the contribution from the $Ni_{1-x}O$ matrix. As represented by the sample fired at 1873 K for 10 h (Fig. 4), the spinel precipitates nucleated predominantly at $Ni_{1-x}O$ dislocations with a line vector parallel to $\langle 1\,0\,0\rangle$ as for pure $Ni_{1-x}O$ (19). In the presence

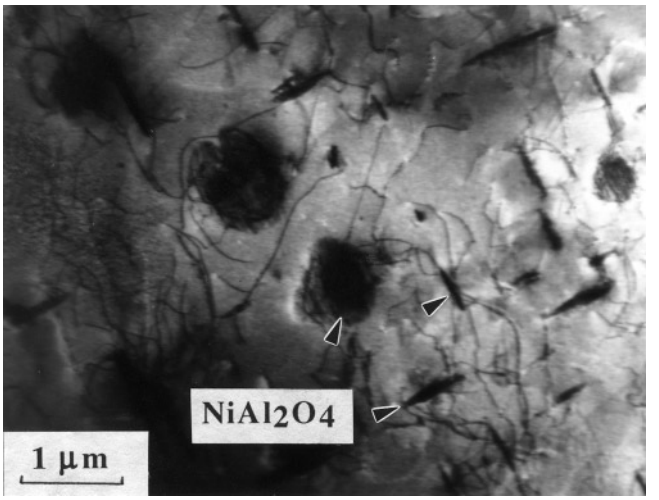

FIG. 3. Bright-field image (BFI) showing three variants of spinel precipitates having a $\{100\}$ habit plane and parallel epitaxy with respect to the $Ni_{1-x}O$ matrix in the [001] zone axis. $N_{69}S_1$ sample fired at 1873 K for 60 h.

of $Ni_{1-x}O$ dislocations, the spinel seeds presumably did not act as growth sites because diffusion distances are smaller than the grain size for the sample. Thermal etching (1723 K for 1 h) of $Ni_{1-x}O$ polycrystals doped with Al^{3+} by reacting with $NiAl_2O_4$ powder at 1873 K for 10 h revealed etch pit opening of the dislocations which have $\{100\}$ ledges and terraces on equally inclined $\{111\}$ walls when viewed along the dislocation line (Fig. 5). Extensive etching at both dislocations and the spinel precipitates caused a mosaic pattern to develop on well-developed $\{100\}$ terraces and ledges.

Lattice images showed that the spinel precipitates had antiphase domain boundaries (APBs) parallel to $\{110\}$. The

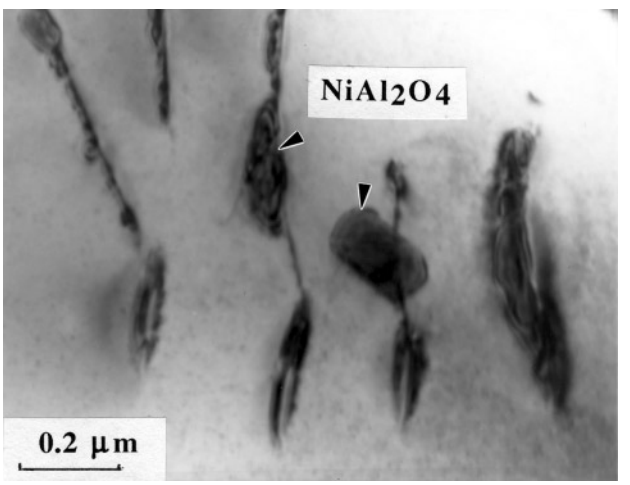

FIG. 4. BFI showing spinel platelets nucleated predominantly at dislocations of the $Ni_{1-x}O$ grain. $N_{69}S_1$ sample fired at 1873 K for 10 h.

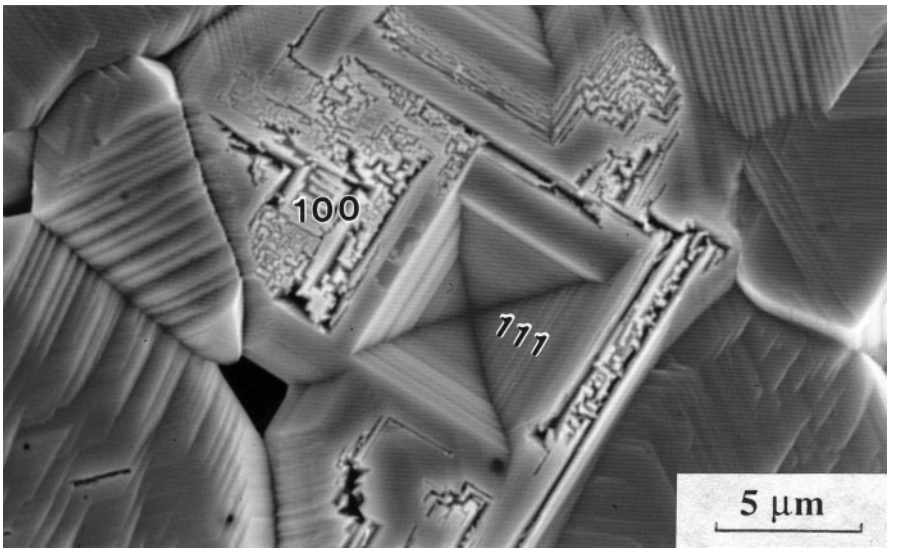

FIG. 5. SEM of $Ni_{1-x}O$ polycrystals doped with Al^{3+} by reacting with $NiAl_2O_4$ powders at 1873 K for 10 h and then thermally etched at 1723 K for 1 h showing etch pit openings with {100} ledges and terraces on inclined {111} walls. Note the accompanied etching at dislocations and spinel precipitates caused a mosaic pattern on {100} terraces.

{111} fringes are offset across the APBs (Fig. 6). The $NiAl_2O_4$ seed also has APBs parallel to {110} as shown by the two-beam image (Fig. 7) for the $N_{69}S_1$ sample fired at 1873 K for 80 h. The interphase interface was found to be zigzag in the presence of {111} facets but coherent with the {111} lattice planes running continuously across the interface (Fig. 8) because the spinel is a $2\times2\times2$ supercell of $Ni_{1-x}O$.

3.2. *Water Quenching*

The TEM study indicated the water-quenched $N_{69}S_1$ sample was free of the spinel precipitates in $Ni_{1-x}O$ grains (not shown); i.e., the Al dopant was not appreciably expelled from the $Ni_{1-x}O$ lattice. The a_0 vs $\cos^2\theta/\sin\theta$ plot of the XRD results further indicated a smaller room temperature lattice parameter (0.4174 nm) for Al-bearing $Ni_{1-x}O$ than

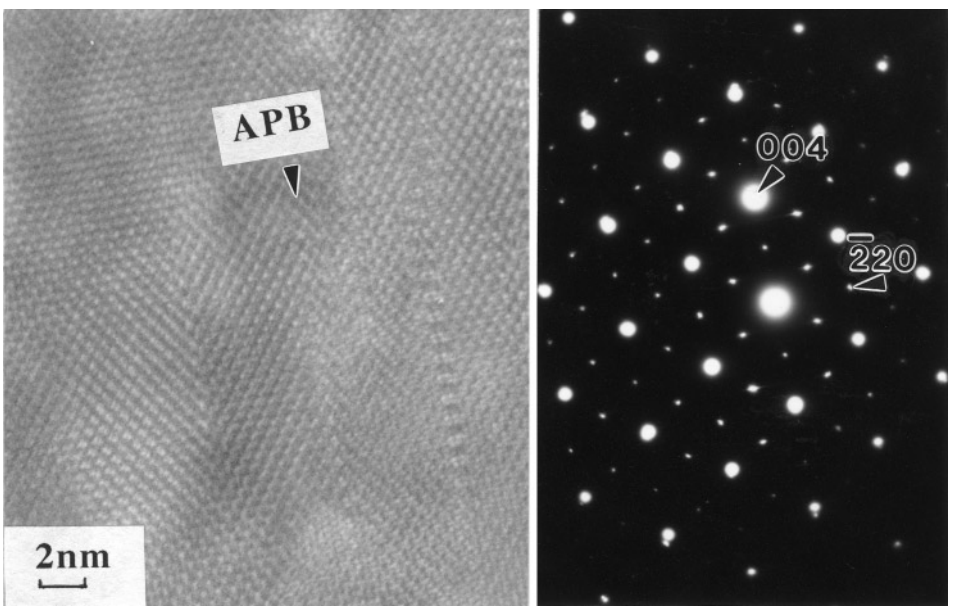

FIG. 6. Lattice image of the spinel precipitate showing antiphase domain boundaries (APBs) parallel to {110} which give rise to diffraction streaks in the SAD pattern. $N_{69}S_1$ sample fired at 1873 K for 60 h.

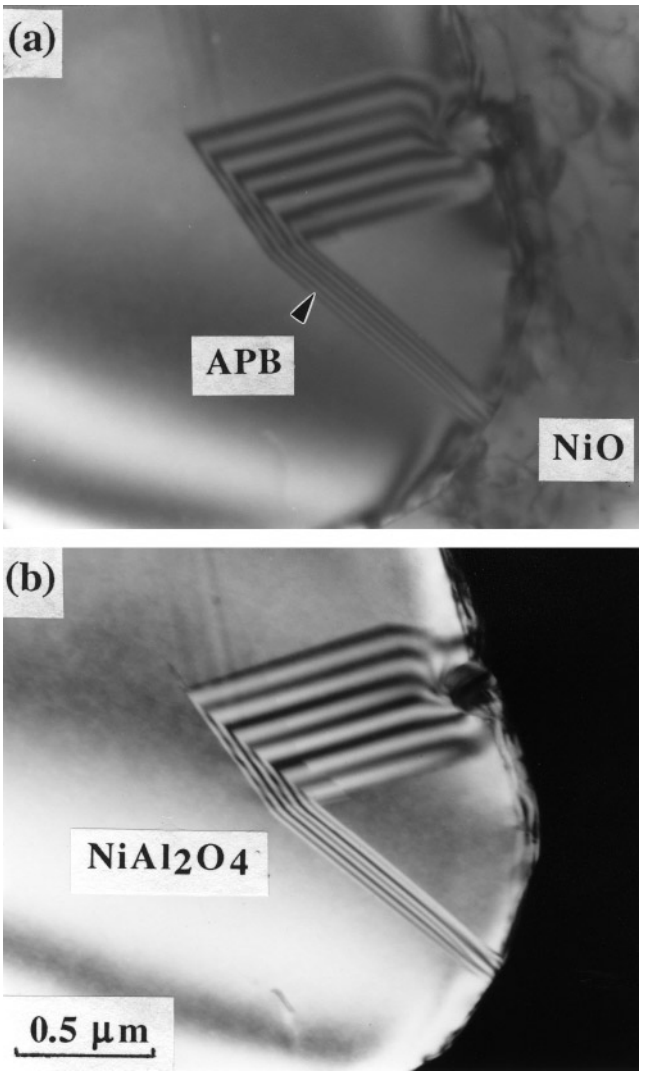

FIG. 7. (a) BFI and (b) DFI with $g = 311$, showing APB of the added $NiAl_2O_4$ particle in $N_{69}S_1$ fired at 1873 K for 80 h.

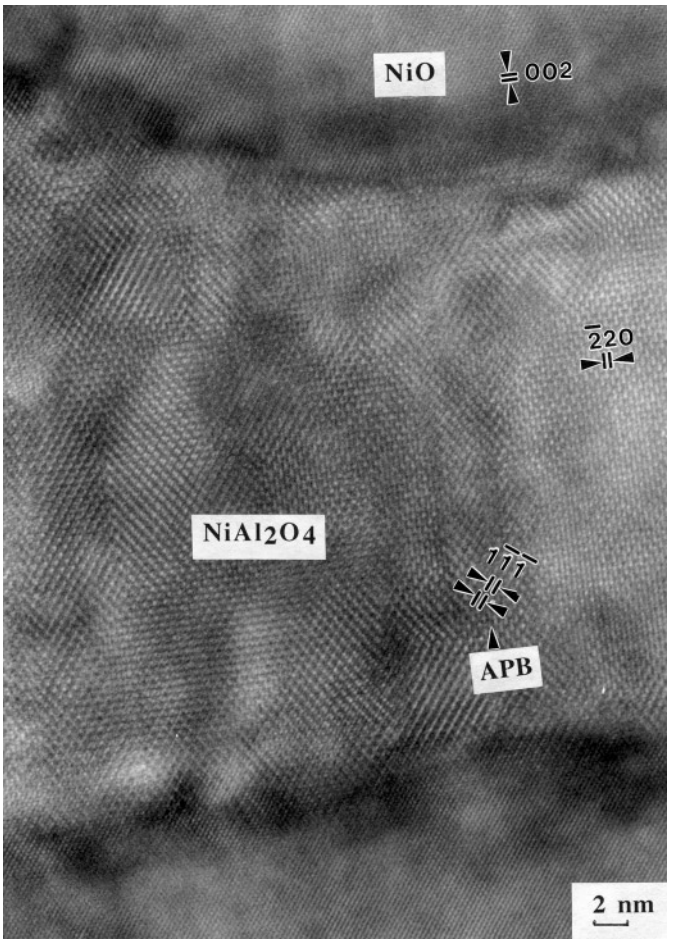

FIG. 8. Lattice image showing {111} planes are coherent across a zigzag {100} habit plane of the spinel platelet. Note also the {111} fringes are offset across the APBs. $N_{69}S_1$ sample fired at 1873 K for 60 h.

Al-free $Ni_{1-x}O$ (0.4177 nm as represented by the furnace-cooled sample). As discussed in Section 4.1, the Al dopant in substitution of Ni at relatively high temperature accounts for a smaller lattice parameter than pure $Ni_{1-x}O$. Thus the spinel precipitates must have been formed by oversaturation during cooling.

4. DISCUSSION

4.1. Defect Chemistry of Al^{3+}-Doped $Ni_{1-x}O$

According to Atkinson *et al.* (17), the nature of "singly charged nickel vacancies" in $Ni_{1-x}O$ is in fact a combination of an electron hole with a conventional Ni vacancy. Presumably, hole localization results in a bound pair of point defects on the Ni sites: $V''_{Ni} + Ni^{3+}Ni^{\bullet}$ in Kröger–Vink notation (21). The implication of Ni^{3+} in contributing to singly charged vacancies is consistent with the change observed in ref 17 toward behavior associated with normal doubly charged vacancies at low pO_2. The charge balance perturbed by the dissolution of Al^{3+} into the $Ni_{1-x}O$ lattice is expected to create atomistic defects, in the form of either $Al^{\bullet}_{Ni}$ or $Al_i^{\bullet\bullet\bullet}$, and be charge compensated by V''_{Ni} or $[V''_{Ni} + Ni^{\bullet}_{Ni}]$ through one or more of the following equations:

$$Al_2O_3 \xrightarrow{NiO} 2Al^{\bullet\bullet\bullet}_{Ni} + 3V''_{Ni} + 3O_O \qquad [I]$$

$$Al_2O_3 \xrightarrow{NiO} 2Al^{\bullet}_{Ni} + V''_{Ni} + 3O_O \qquad [II]$$

$$Al_2O_3 \xrightarrow{NiO} 2Al_i^{\bullet\bullet\bullet} + 6[V''_{Ni} + Ni^{\bullet}_{Ni}] + 3O_O \qquad [III]$$

$$Al_2O_3 \xrightarrow{NiO} 2Al^{\bullet}_{Ni} + 2[V''_{Ni} + Ni^{\bullet}_{Ni}] + 3O_O \qquad [IV]$$

It should be noted, however, that larger clusters may be necessary to explain the low diffusivity of defects in

Al-doped NiO (17). In any case, Al^{3+} residing in the interstitial sites of $Ni_{1-x}O$, i.e., through Eqs. [I] and [III], are more effective in increasing nickel vacancies.

At temperatures above 1473 K, the Ni tracer diffusion data have been shown to fit a model in which singly charged (rather than doubly charged) V–Ni^{3+} pairs form associates with Al dopant ions with a binding energy of 1.2 eV; i.e., (17)

$$NiAl_2O_4 + \tfrac{1}{2}O_2 \rightarrow NiO + 2Al_{Ni}^{\bullet} + 2[V''_{Ni} + Ni_{Ni}^{\bullet}] + 4O_O \quad [V]$$

Given that the ionic radius of Al^{3+} (0.0535 nm) is smaller than that of Ni^{2+} (0.069 nm) or Ni^{3+} (0.060 nm, high spin) in an octahedral site (22), the Al-doped $Ni_{1-x}O$, as retained by water quenching, has a smaller room temperature lattice parameter than pure $Ni_{1-x}O$. The cell parameter for pure $NiAl_2O_4$ (0.8048 nm) is less than twice that of $Ni_{1-x}O$, indicating also that octahedral contraction is indeed the predominant effect. However, it is possible that large O–O distances associated with interstitial tetrahedral Al could somehow compensate for the contraction on octahedral sites. Reaction [V] did not cause the formation of a paracrystalline state as indicated by prolonged (80 h) annealing of the present composite at 1873 K.

Below 1473 K, we suggest that the point defects produced due to Al dopant may form 4:1 defect clusters with four octahedral Ni vacancies (singly charged V–Ni^{3+} pairs) surrounding a dopant tetrahedral interstitial through the following equation:

$$Al_{Ni}^{\bullet} + 2V''_{Ni} + 2Ni_{Ni} \rightarrow [Al_i^{\bullet\bullet\bullet} + 4V''_{Ni} + 4Ni_{Ni}^{\bullet}] \quad [VI]$$

This reaction is based on the fact that the $NiAl_2O_4$ spinel falls into the inverse type with Al in both tetrahedral and octahedral sites but Ni restricted to octahedral sites (23). Note that trivalent transition metal dopant (D) was suggested to stabilize 4:1 defect clusters (the spinel precursor) with four octahedral Ni vacancies (doubly charged rather than singly charged) surrounding a dopant tetrahedral interstitial (24); i.e.,

$$D_{Ni}^{\bullet} + 3V''_{Ni} + 5Ni_{Ni}^{\bullet} \rightarrow D_i^{\bullet\bullet\bullet} + 4V''_{Ni} + 5Ni_{Ni}^{\bullet} \quad [VII]$$

Singly charged V–Ni^{3+} pairs are likely predominant for reaction [VI] below 1473 K, because under specified oxygen partial pressure, the $[V''_{Ni}]/[V'_{Ni}]$ ratio (<1) decreases with decreasing temperature over the range 1273–1973 K and V''_{Ni} diffuses with a smaller activation enthalpy than V'_{Ni} (25).

It should be emphasized that spinel does not exsolve from $Ni_{1-x}O$ saturated with $NiAl_2O_4$ at 1873 K until 1473 K. Presumably, incorporation of Al in solid solution may take place by a reaction such as [V], and moving Al into interstitial sites as in reaction [VI] is a likely precursor to spinel nucleation. The equilibrium behavior of Al-saturated $Ni_{1-x}O$ would be predicted to involve continuous exsolution of $NiAl_2O_4$ with decreasing temperature. The observation that precipitation only actually occurs at 1473 K is consistent with the idea that nucleation requires the change in defect type at this temperature as deduced from the diffusivity measurements of ref (17).

4.2. *Nucleation Mechanism of Al^{3+}-Doped $Ni_{1-x}O$*

The existence of APBs in the spinel platelet indicates a multiple nucleation event at lattice sites, presumed to be triggered by Al moving from octahedral to tetrahedral sites below 1473 K via Eq. [VI]. The APBs probably have rather low energy and the local structure is necessarily of the "spinelloid" type with corner-linked tetrahedra. The $NiAl_2O_4$–Ni_2SiO_4 system is known to include several such structures, which occur at intermediate compositions as both stable macroscopic phases and unit cell-scale intergrowths (26).

Given the parallel orientational relationship between the spinel platelets and the $Ni_{1-x}O$ matrix, no transformation twin variants of spinel are allowed. Nucleation at dislocations with $\langle 001 \rangle$ line vectors, known to occur in $Ni_{1-x}O$, is consistent with the observed precipitates of spinel as coherent $\{001\}$ platelets. In addition, a coherent interphase interface is in accordance with the nucleation event at dislocations (27). The dislocations may act as a source of nickel vacancies, hence facilitating the formation of 4:1 clusters and ultimately spinel nuclei.

Theoretical calculations indicated that nickel vacancy concentration increased by a factor of about 40 over the bulk value for the (211)/[011] twist grain boundary of $Ni_{1-x}O$ at 1000 K (28). The relaxation in this distorted region of boundary or, analogously, the dislocation cores is expected to affect binding of point defects. Although the knowledge of the core structure of dislocations and the interaction of point defects with dislocations in most oxides is virtually nil (cf. Mitchell *et al.* (29)), atomistic calculations of point-defect interactions with an edge dislocation in NiO indicated that doubly charged nickel vacancies have a lower binding energy than singly charged vacancies (30). In addition, it is well established that impurities preferentially adsorb on dislocation outcrops and hence affect the incubation time of etch pits (ref 31 and literature cited therein). It is noteworthy that Ni self-diffusion along dislocations is important at temperatures below 1073 K (32), but oxygen self-diffusion along dislocations relative to in-bulk material appears significant at temperatures as high as 1473 K (33). Thus dislocations have a beneficial high diffusivity of atoms for the nucleation process.

It should be noted that unlike wüstite (6), (Zr, Y)-codoped $Ni_{1-x}O$ (15, 16), or Zr-doped $Ni_{1-x}O$ (16), which have the 4 : 1 defect clusters arranged as a paracrystalline state before transforming into the spinel phase, the present Al^{3+}-doped $Ni_{1-x}O$ transforms directly into the spinel phase below 1473 K. It remains to be studied whether the dopant dependence of binding energy, the correlation factor, or the migration energy terms affect the transformation route.

It might also prove worthwhile to study the possible transformation of analogous systems, e.g., Al-doped MgO, from the foregoing point of view. It is of interest to know if Al^{3+} favors both the interstitial tetrahedral site and the octahedral site, as for inverse-type spinel, or only the octahedral site, as for the case of normal-type spinel (23). In the latter case, the dopant cation might well avoid the interstitial site and hence not form 4 : 1 clusters.

4.3. Energetics of Interphase Interface

The spinel precipitate has a {100} habit plane due to the control of nucleation sites, i.e., dislocations with the ⟨100⟩ line vector. However, the {100} interface is not very planar in the lattice image (Fig. 8) because of the development of {111} facets. Thermal etching at dislocation outcrops also showed well-developed {111} walls with {100} ledges (Fig. 5). In fact, in the spinel phase, {111} is known to have a lower surface energy than {100} (34). In pure NiO or NiO-rich NiO–MgO solid solution, the {111} facets are also more stable than {100} (35, 36). The oxygen sublattice probably remained relatively inert during the transformation because of a much lower diffusivity of oxygen than Ni (ca. four orders of magnitude difference at 1873 K) (33)), in accordance also with the fact that oxygen close-packed {111} planes are continuous across the interphase interface.

Note the room temperature X-ray lattice parameters are 0.8048, 0.4177, and 0.4174 nm for $NiAl_2O_4$ spinel, $Ni_{1-x}O$, and Al-doped $Ni_{1-x}O$, respectively. The lattice mismatch (δ) is calculated to be small (0.07) and is consistent with the formation of a coherent interphase interface {100} with ledges. Since the $NiO \cdot nAl_2O_3$ spinel follows the lattice parameter vs composition relationship $a_n = a_1 - 0.077(n-1)$ in the spinel phase field (16), an even smaller lattice mismatch with respect to $Ni_{1-x}O$ is expected if the spinel precipitate has $n < 1$ and the extrapolation of the foregoing equation is valid. On the other hand, surface energy effects, expected to be pronounced in the nucleation stage, might raise the free energy–composition curve of the spinel solid solution, giving an Al-rich ($n > 1$) local equilibrium composition for the spinel and a larger lattice mismatch. Dislocation cores, having a relatively more open structure than the lattice, are favorable in minimizing the lattice misfit strain energy—hence the lower activation energy for nucleation.

5. CONCLUSIONS

1. Expulsion of Al^{3+} during slow cooling of Al-doped $Ni_{1-x}O$ caused the formation of stoichiometric $NiAl_2O_4$ precipitates which have {110} antiphase domain boundaries of a spinelloid nature and are of the same size regardless of the firing time at 1873 K. The precipitate size may well be dependent on cooling rate.

2. Preferential nucleation on dislocations is demonstrated despite the presence of spinel seeds. Presumably, the seeds do not act as growth sites because diffusion distances are smaller than the grain size of the samples, given the annealing temperature and cooling rates of this study. The interface is coherent because the lattice parameters of the spinel and $Ni_{1-x}O$ are closely commensurate.

3. On the basis of diffusion data reported by Atkinson *et al.* (17) for Al-doped $Ni_{1-x}O$ single crystals, we suggest that below 1473 K, moving of some Al^{3+} dopant from octahedral to interstitial tetrahedral sites caused the spinel nucleation.

ACKNOWLEDGMENT

We thank an anonymous referee for helpful comments.

REFERENCES

1. B. E. F. Fender and F. D. Riley, "The Chemistry of Extended Defects in Non-Metallic Solids" (L. Eyring and M. O'Keefe, eds.). North-Holland, Amsterdam, 1970.
2. C. R. A. Catlow and B. E. F. Fender, *J. Phys. C: Solid State Phys.* **8,** 3267 (1975).
3. P. Vallet and P. Raccah, *Mem. Sci. Rev. Metall.* **62,** 1 (1965).
4. B. Andersson and J. O. Sletnes, *Acta Crystallogr., Sect. A* **33,** 268 (1977).
5. J. Manenc, J. Bourgeot, and J. Benard, *C. R. Acad. Sci. Paris* **258,** 4528 (1964).
6. T. R. Welberry and A. G. Christy, *J. Solid State Chem.* **117,** 398 (1995).
7. H. G. Sockel and H. Schmalzried, *Ber. Bunsenges. Phys. Chem.* **72,** 745 (1968).
8. C. R. A. Catlow and A. M. Stoneham, *J. Am. Ceram. Soc.* **64,** 234 (1981).
9. R. W. Grime, A. B. Anderson, and A.H. Heuer, *J. Am. Ceram. Soc.* **69,** 619 (1986).
10. C. M. Osburn and R. W. Vest, *J. Phys. Chem. Solids* **32,** 1331 (1971).
11. R. L. Lalauze and J. H. Meunier, *Oxid. Met.* **12,** 183 (1978).
12. W. C. Tripp and N. M. Tallan, *J. Am. Ceram. Soc.* **53,** 531 (1970).
13. M. L. Volpe and J. Reddy, *J. Chem. Phys.* **53,** 1117 (1970).
14. J. Szuber, *J. Mater. Sci.* **19,** 1991 (1984).
15. P. Shen, S. Chen, and H. S. Liu, *Mater. Sci. Eng., A* **161,** 135 (1993).
16. J. Chen, Ph.D. Thesis, National Sun Yat-sen University, Taiwan, 1996.
17. A. Atkinson, A. E. Hughes, and A. Hammou, *Philos. Mag. A* **43,** 1071 (1981).
18. G. Remaut, P. Delavignette, A. Lagasse, and S. Amelinckx, *Phys. Status Solidi* **11,** 329 (1965).
19. B. D. Cullity, "Elements of X-ray Diffraction." Addison-Wesley, Reading, MA, 1978.
20. S. R. Wang, M.S. Thesis, National Sun Yat-sen University, Taiwan, 1996.

21. F. A. Kröger and H. J. Vink, *Solid State Phys.* **3,** 307 (1956).
22. R. D. Shannon, *Acta Crystallogr., Sect. A* **32,** 751 (1976).
23. M. T. Weller, *in* "Inorganic Materials Chemistry," p. 60. Oxford University Press, New York, 1994.
24. R. W. Grime, A. B. Anderson, and A. H. Heuer, *J. Phys. Chem. Solids* **48,** 45 (1987).
25. N. L. Peterson and C. L. Wiley, *J. Phys. Chem. Solids* **46,** 43 (1985).
26. G. D. Price, *Phys. Chem. Miner.* **10,** 77 (1983).
27. D. A. Porter and K. E. Easterling, "Phase Transformation in Metals and Alloys," Van Nostrand Reinhold Co., New York, 1981.
28. D. M. Duffy, *Philos. Mag.* **50,** 143 (1984).
29. T. E. Mitchell, L. W. Hobbs, A. H. Heuer, J. Castaing, J. Cadoz, and J. Philibert, *Acta Metall.* **27,** 1677 (1979).
30. J. Rabier, J. Soullard, and M. P. Puls, *Philos. Mag. A* **61,** 99 (1990).
31. C. C. Lin and P. Shen, *Geochim. Cosmochim. Acta* **59,** 2955 (1995).
32. A. Atkinson and R. I. Taylor, *Philos. Mag. A* **39,** 581 (1979).
33. C. Dubois, C. Monty, and J. Philibert, *Philos. Mag. A* **46,** 419 (1982).
34. P. Shen, S. Chen, and W. S. Chang, *Mater. Sci. Eng., A* **184,** L5 (1994).
35. C. A. Handwerker, M. D. Vaudin, and J. E. Blendell, *J. Phys., Colloq.* **5,** 367 (1988).
36. J. W. Cahn and C. A. Handwerker, *Mater. Sci. Eng., A* **162,** 83 (1993).